HHS Public Access

Author manuscript

Adv Mater. Author manuscript; available in PMC 2019 April 01.

Published in final edited form as:

Adv Mater. 2018 April ; 30(16): e1707306. doi:10.1002/adma.201707306.

Design and Fabrication of a Hierarchically Structured Scaffold for Tendon-to-Bone Repair

Dr. Chunlei Zhu,
The Wallace H. Coulter Department of Biomedical Engineering, Georgia Institute of Technology and Emory University, Atlanta, GA 30332, USA

Dr. Suphannee Pongkitwitoon,
Department of Orthopaedic Surgery, Columbia University, New York, NY 10032, USA, Department of Biomedical Engineering, Columbia University, New York, NY 10027, USA

Dr. Jichuan Qiu,
The Wallace H. Coulter Department of Biomedical Engineering, Georgia Institute of Technology and Emory University, Atlanta, GA 30332, USA

Prof. Stavros Thomopoulos, and
Department of Orthopaedic Surgery, Columbia University, New York, NY 10032, USA, Department of Biomedical Engineering, Columbia University, New York, NY 10027, USA

Prof. Younan Xia
The Wallace H. Coulter Department of Biomedical Engineering, Georgia Institute of Technology and Emory University, Atlanta, GA 30332, USA, School of Chemistry and Biochemistry, School of Chemical and Biomolecular Engineering, Georgia Institute of Technology, Atlanta, GA 30332, USA

Abstract

A hierarchically structured scaffold is designed and fabricated for potentially facilitating the tendon-to-bone repair. The scaffold is comprised of three regions with distinct functions: *i*) an array of channels to guide the in-growth of cells and aligned deposition of collagen fibers, as well as integration of the scaffold with the tendon side, *ii*) a region with a gradient in mineral composition to facilitate stress transfer between tendon and bone, and *iii*) a mineralized inverse opal region to promote the integration of the scaffold with the underlying bone. Cell culture experiments confirm that adipose-derived stromal cells are able to infiltrate and proliferate through the entire thickness of the scaffold without compromised cell viability. The seeded stem cells exhibit directed differentiation into tenocytes and osteoblasts along the mineral gradient as a response to the graded Young's modulus. This novel scaffold holds great promise to promote a functional tendon-to-bone attachment by offering a structurally and compositionally appropriate microenvironment for healing.

younan.xia@bme.gatech.edu.

Supporting Information

Supporting Information is available from the Wiley Online Library or from the author.

Keywords

hierarchically structured scaffold; inverse opal; tendon-to-bone insertion; tissue engineering; regenerative medicine

To achieve joint motion, muscle forces are transferred to bone across an intricate tendon-to-bone attachment site known as the enthesis.[1] The attachment is hierarchical, including gradations in mineral content,[2–4] interdigitation of collagen fibers,[5] and a toughening band of compliant matrix,[6,7] to facilitate the dissipation of stresses across the interface. This complex transitional tissue is not regenerated after injury, with a healing process that is driven by scar formation (*i.e.*, poorly organized collagen deposition) and bone loss.[8] The lack of a functionally graded transition at the healing interface results in stress concentrations because of the structural mismatch between tendon and bone, contributing to high failure rates after surgical repair (*e.g.*, failure rates after rotator cuff surgical repairs range from 20 to 94%, depending on the patient population).[6,9] There is a clinical need for tissue-engineering approaches to promote regeneration of the native interface and reduce the poor outcomes after tendon-to-bone repair.

Toward this end, the design and fabrication of biomimetic scaffolds have received great attention in tissue engineering and regenerative medicine.[6,10–12] Among the many types of scaffolds that have been created for use in tendon-to-bone repair, those with a biphasic, triphasic or continuously-graded structures comprised of both non-calcified and calcified regions have shown the greatest promise.[13–18] These biomimetic scaffolds recapitulate some aspects of the native tendon-to-bone attachment, promoting better healing and functional recovery. However, despite impressive progress in the design and fabrication of such scaffolds, their applications *in vivo* have remained limited, primarily due to low cell loading capacity and uneven distribution, indirect application to the interface, or a mismatched length scale of the mineral gradient. To address these issues, we developed a novel class of three-dimensional (3D) scaffolds to facilitate tendon-to-bone regeneration.

A biomimetic approach was taken to design hierarchical scaffolds for tendon-to-bone repair. At the native enthesis, effective attachment is achieved between tendon and bone *via*: a mineral gradient on the order of tens of micrometers,[2–4] collagen fibers inserting across a wavy interdigitation geometry on the order of hundreds of micrometers,[5,19] and a trabecular bony foundation on the order of thousands of micrometers.[2] Here we report the design, fabrication, and evaluation of a hierarchically structured scaffold that recapitulates anatomic structure of the tendon-to-bone attachment site (Scheme 1). Two FDA-approved materials, hydroxyapatite (HAp)[20] and poly(lactic-*co*-glycolic acid) (PLGA),[21] were used to construct the scaffold. To create a porous, rigid structure comparable to trabecular bone, HAp/PLGA composite was infiltrated into the void space among gelatin beads (*ca.* 220 μm in diameter) in an opaline lattice. To generate an interface comparable to the graded enthesis, a layer-by-layer coating strategy was used to generate a mineral gradient along the layering direction over a tunable distance of 25−50 μm. To support the formation of an aligned, unmineralized extracellular matrix and interconnect the three phases, an array of channels (*ca.* 150 μm in diameter and separated by *ca.* 140 μm) were machined using a CO_2 laser. The

final hierarchical scaffold was obtained by dissolving the gelatin beads in warm water. Since cells are responsive to both substrate composition and stiffness,[22,23] the hierarchically structured scaffold has the potential to stimulate the differentiation of stem cells and guide the synthesis of appropriate extracellular matrix and mineralization. Notably, the natural tendon-to-bone attachment is a functionally graded structure. In addition to the mineral gradient, a variety of other properties also exhibit spatial variations, such as extracellular matrix composition (*e.g.*, collagen type and proteoglycan content) and cell phenotypes. However, the origin of failure for rotator cuff-related surgery lies in the poor healing process that is typically characterized by bone loss and scar formation, where the lack of graded mineral content and poorly organized collagen fibers results in a mechanically weak attachment.[18] To this end, the emphasis of this study was focused on the establishment of a gradient in mineral content as well as the control of scaffold microstructure.

The voids in an opaline lattice of gelatin beads were first infiltrated with a homogeneous HAp/PLGA solution according to our previously reported method.[24] Since pores with sizes in the range of 100−400 μm are optimal for bone regeneration,[25] we chose 220-μm gelatin beads as the sacrificial template. The HAp/PLGA-infiltrated scaffold was *ca.* 1 mm in height, with a diameter of *ca.* 4 mm at the top surface and *ca.* 5 mm at the base surface. Removal of the gelatin beads revealed that the HAp/PLGA inverse opal structure had an array of uniform pore sizes of *ca.* 200 μm in the bulk (<220 μm due to solvent evaporation), together with interconnecting windows of 40−50 μm in size (Figure S1A, Supporting Information). Both the uniformity and interconnectivity of the pores play important roles in facilitating cell adhesion, migration, and distribution, as well as efficient transportation of oxygen/nutrients and metabolite wastes.[26] Due to the incorporation of HAp nanoparticles, the surface of the structure became rough and was characterized by a large number of nanoscale bumps (Figure S1B, Supporting Information).

The gradient in mineral content at the tendon-to-bone insertion spans across a distance of *ca.* 20−60 μm, regardless of species.[4] Therefore, a new strategy was developed for generating a mineral gradient on a comparable length scale. Specifically, a series of 16 wt.% PLGA solutions with varying HAp concentrations were used to coat the top surface of an opaline lattice (after infiltration with homogeneous HAp/PLGA) in a layer-by-layer manner, including 15 wt.% HAp for the first two layers, 10 wt.% HAp for the third layer, and 5 wt.% HAp for the fourth layer. In addition, three layers of pure 16 wt.% PLGA were added to form a non-calcified region. The as-prepared scaffold with graded mineral content was then cryo-sectioned along the vertical direction for characterization *via* energy-dispersive X-ray spectroscopy (EDX). As anticipated, the transitional area (with a thickness of *ca.* 37 μm) exhibited graded changes in both calcium and carbon contents (Figure 1A−C). The calcium gradually decreased from the bottom layer to the top layer, whereas the carbon showed an opposite trend. Such a graded change was further quantified by dividing the interface into ten small sections. As shown in Figure 1D, the ratio of Ca/(C+Ca) exhibited a gradual decrease from *ca.* 8% at the bottom layer to 0% at the top layer. This result was consistent with a gradual decrease in HAp, suggesting the successful establishment of a controlled mineral gradient.

We next focused on the generation of an array of uniaxially aligned channels to guide the infiltration of cells and the deposition of properly aligned collagen fibers. To this end, a 10.6 μm-CO_2 laser with a beam size of 200 μm was used to pattern the graded HAp/PLGA film. An array of 10×10 channels were created over an area of 2.5 mm × 2.5 mm (Figure S2A, Supporting Information). Based on the SEM image in Figure S2B of the Supporting Information, the average opening at the top surface and separation between the openings were determined to be 154 ± 8 and 127 ± 8 μm, respectively. The size of each opening was compatible to the dimensions of cells (20−60 μm) and collagen fascicles (50−400 μm), consistent with the anatomy of tendon.[27] As a result, tenocytes would be expected to easily infiltrate and deposit collagen inside these channels. Furthermore, a number of smaller pores (20−40 μm) were formed around the channels during laser machining (Figure S2C, Supporting Information), which can be attributed to the bubbling of PLGA during laser ablation. To gain more insight into the structure of an individual channel, the cross-section of a laser-machined scaffold was examined using SEM. As shown in Figure S2D of the Supporting Information, the CO_2 laser was able to pass through the HAp/PLGA film and reach the gelatin beads, making the three regions of the scaffold interconnected. The average depth of the channels was 301 ± 12 μm, with the HAp/PLGA film accounting for 127 ± 11 μm (including a graded interface of 37 ± 8 μm).

The gelatin beads were then dissolved in warm water to reveal the porous structure of the trabecular region in the scaffold. As shown in Figure 2A, all channels were retained during template removal and no significant changes to the morphology was observed. Based on the SEM image shown in Figure 2B, the average diameter of the openings at the top surface was 146 ± 9 μm, with the separation between openings being 139 ± 12 μm. These data suggest that the removal of gelatin template only had a minimal impact on the scaffold geometry. Besides the large (*ca.* 150 μm) and small (*ca.* 30 μm) pores generated during laser machining, additional smaller pores were formed in the interior of the PLGA layer, with diameters ranging from 0.9 to 7 μm upon removal of the gelatin beads (Figure 2C,D and Figure S3, Supporting Information). These newly formed pores likely originated from the residual 1,4-dioxane encapsulated in the viscous PLGA during solvent evaporation. This was verified by soaking a mineral-graded film deposited on a silicon wafer in warm water (Figure S4, Supporting Information). Since 1,4-dioxane is miscible with water and PLGA has a low glass transition temperature around 37 °C,[21] the scaffold could slightly deform to favor the escape of residual solvent, leaving behind a porous structure. After template removal, the inverse opal base showed interconnected windows between adjacent pores, and the escape of residual solvent resulted in an increase in height for the HAp/PLGA film to 156 ± 14 μm (Figure 2D). Meanwhile, the escape of solvent also contributed to a close packing for the HAp nanoparticles, leading to a decrease for the graded interface (27 ± 6 μm). The same trend was also observed in the mineral-graded film deposited on a silicon wafer (Figure S4, Supporting Information). Nevertheless, the mineral gradation at the interface was well retained, as confirmed by EDX mapping (Figure S5, Supporting Information). It should be emphasized that the length scale of the graded interface can be easily extended to generate a graded interface to exactly match the length scale of any clinically relevant enthesis (*e.g.*, up to 100 μm),[4] providing a structure that can maximally recapitulate the native mineral interface between tendon and bone.

The incorporation of a stiff mineral in compliant PLGA is expected to stiffen the resulting composite. To validate this argument for the hierarchically structured scaffold, we examined the local modulus along the mineral gradient using atomic force microscopy (AFM), a tool capable of mechanical indentation testing, imaging, and nanoscale manipulation.[28,29] Briefly, the AFM tip was guided over a specific area *via* a laser system. The force and vertical displacement were derived from the drive amplitude to indent the scaffold and the lateral deflection amplitude of the cantilever, respectively. The ratio of force to vertical displacement in the linear portion of the force-displacement curve was used to determine the Young's modulus according to the Hertz model. As shown in Figure 3, there was a strong correlation between the local Young's modulus and mineral content. Specifically, the Young's modulus increased monotonically as the amount of HAp increased along the mineral gradient. The modulus on the unmineralized region was on the order of 200 MPa (location #1), whereas the modulus on the highly-mineralized region was on the order of 2 GPa (location #7). In this scaffold, the doping of PLGA by HAp resulted in a 10-fold increase in the Young's modulus. Such a mineral-graded interface is promising for dissipating stress concentrations between two dissimilar tissues and reproduces a critical feature of the natural tendon-to-bone attachment (where the modulus changes from 200 MPa for the compliant tendon to 20 GPa for the relatively stiff bone).[6] Although the modulus of the unmineralized region of the scaffolds is in good accordance with native tendon, the modulus of the highly-mineralized region is still one order of magnitude lower than that of bone. This gap could potentially be alleviated through subsequent mineralization by the osteoblasts derived from the seeded stem cells.

To investigate the distribution and proliferation of cells inside the scaffold, adipose-derived stromal cells (ASCs), a promising mesenchymal stem cell capable of differentiating into multiple cell lineages, were seeded and cultured in the scaffold.[30,31] To examine the cell distribution along the vertical direction, the ASC-seeded scaffold was cryo-sectioned and stained with fluorescent dyes for imaging. As shown in Figure 4A, ASCs were able to infiltrate into the entire scaffold, with the top surface close to the aligned channels having the largest cell number. The relatively large cell number at the top surface is attributed to the sedimentation of excess ASCs during cell seeding. In the inverse opal region, however, ASCs were uniformly distributed, indicating that the cells proliferated and freely migrated within the porous structure. This feature may be advantageous, as interconnectivity plays a crucial role in promoting cell interactions and communication during tendon-to-bone healing.[2,26] To quantify cell distribution, the scaffold was divided into three sections for analysis, including the aligned channels (AC), the upper part of the inverse opal (IO-U), and the lower part of the inverse opal (IO-L). As shown in Figure 4B, during 7 days of culture, the relative number of ASCs in each of the three regions did not change, with values of *ca.* 40%, 30%, and 30% for the AC, IO-U, and IO-L, respectively, indicating that the ASCs proliferated at a constant rate in all regions. Interestingly, the ASCs in the inverse opal region became more rounded at days 4 and 7 relative to those at day 1 (see magnified images in Figure 4A). However, the cells in the top surface of the scaffold retained a highly-elongated morphology. The rounded cells in the inverse opal region was further quantified. Figure 4C shows that as incubation was prolonged, the ratio of rounded cells gradually increased, changing from *ca.* 10% to *ca.* 35%. The change in cell shape may indicate a

variation to the cell phenotype in response to the local concentration of HAp owing to its high osteoinductivity and osteoconductivity.[24,32,33]

The cell viability inside the scaffolds was then analyzed using modified live/dead staining. During the 7 days of culture, the ASCs maintained high viability, with negligible death (Figure S6A, Supporting Information). When examining cell survival rate, from day 1 to 7, the ASCs had a survival rate of >90%, suggesting excellent biocompatibility of the hierarchical scaffold (Figure S6B, Supporting Information). The uniformity and interconnectivity of the scaffold may facilitate efficient exchange of oxygen/nutrients and metabolite wastes, giving rise to the high cell viability. In addition, we performed the 3-(4,5-dimethylthiazol-2-yl)-2,5-diphenyltetrazolium bromide (MTT) assay to evaluate the proliferation of ASCs inside the scaffold. As shown in Figure S6C of the Supporting Information, the absorbance values of the cultures at days 1, 4 and 7 were 0.20 ± 0.03, 0.55 ± 0.05, and 0.95 ± 0.01, respectively, indicating that the ASCs in the hierarchical scaffold exhibited a linear increase in proliferation throughout the 7 days of culture. The 3D porous structure had more space to accommodate implanted cells compared to a 3D non-porous scaffold or a 2D scaffold, which is an important consideration for *in vivo* application. These data indicate that the hierarchical scaffold can support uniform seeding of cells and provide an environment that promotes cell viability and proliferation.

To understand the influence of the mineral gradient and scaffold microstructure on ASC differentiation, we evaluated both tenogenesis and osteogensis. After 28 days of culture, cross sections of the scaffold were obtained to examine cell differentiation along the mineral gradient. Immunocytochemistry was then performed to fluorescently visualize scleraxis (Scx) and runt-related transcription factor 2 (Runx2), which are the tendon-specific marker and an early marker of osteogenic differentiation, respectively.[34,35] As shown in Figure 5, from the unmineralized region to the highly-mineralized region, an opposing pattern for tenogenesis and osteogenesis was observed. The expression of Scx was dominated in the top unmineralized region, suggesting the preferential differentiation of ASCs into the tenogenic lineage in the area composed of pure PLGA (Figure 5A). As for the transitional regions, both the expression of Scx and Runx2 could be found, in which the transitional region with less mineral content showed more Scx (Figure 5B), whereas the transitional area with more mineral content showed more Runx2 (Figure 5C). The regions with multiple cell lineages may be critical for promoting enthesis regeneration *via* heterotypic cellular interactions.[6] In the bottom mineralized region, the expression of Runx2 was higher than Scx, suggesting the preferential differentiation of ASCs into the osteogenic lineage in the area with the highest amount of minerals (Figure 5D). To further evaluate these expression patterns, we performed semi-quantitative analysis of Scx and Runx2 expressions based on the mean pixel intensities of each image. As expected, there was a graded change in the expressions of both Scx (gradually decreasing with increasing mineralization) and Runx2 (gradually increasing with increasing mineralization) (Figure 5E,F). These data demonstrate that the hierarchically structured scaffolds with mineral gradients were able to facilitate local stem cell differentiation and that process was highly dependent on local mineral content and substrate stiffness.

It should be noted that the goal of the immunocytochemistry assay we used was to demonstrate the spatially graded differentiation pattern of stem cells on the scaffolds. Numerous markers for tenogenesis and osteogenesis can be used to identify the cells along the early-to-late differentiation path. In this study, we chose Scx to identify tenogenic differentiation because it is a transcription factor associated with cells differentiating into tendon fibroblasts[36] and is also a lineage-specific marker for tenogenesis.[37] We chose Runx2 to identify osteogenesis because it is a transcription factor specific for cells differentiating into osteoblasts and is also a lineage-specific marker for osteogenesis.[38] These early markers of differentiation imply progress toward tenogenesis or osteogenesis.[39] Confirmation of fully differentiated tendon fibroblasts and fully differentiated osteoblasts is often done by examining collagen deposition using picrosirius red staining[40] and calcification using alizarin red staining,[41] respectively. However, monitoring collagen deposition by picrosirius red or calcification by alizarin red may demonstrate the functionality of the cell and the cell maturity, implying a later stage of stem cell differentiation, but does not necessarily demonstrate stem cell differentiation towards a specific lineage. Moreover, these assays are non-specific, as positive staining can also be found in non-differentiated stem cells[42] and other fully differentiated cells (*e.g.*, cardiac cells, hepatocytes, alveolar cells, and bronchial cells[43–45]). In addition, although techniques such as quantitative polymerase chain reaction (qPCR) would allow for examination of a large number of genes, the approach would require a large number of cells and cell removal from the micrometer-scale gradient mineralized area in the scaffold; these issues would limit our ability to determine localized expression patterns along the mineral gradient. One way to achieve this would be to section the scaffold. However, sectioning of unfixed scaffolds is difficult, prone to artifacts and fragmenting, and does not result in accurate separation of graded regions. Unfortunately, both fixation of cells and subsequent processing for frozen sections generally alter the structures of RNA and/or DNA, leading to unreliable gene expression measurements.[46,47] As such, we limited our approach to qualitative and semi-quantitative immunocytochemistry-based outcomes, specifically mapping the spatially graded patterns of a tendon-specific differentiation marker (Scx) and a bone-specific differentiation marker (Runx2).

In summary, we have demonstrated the fabrication of a hierarchically structured scaffold with promise for the repair of tendon-to-bone insertion. The scaffold contained three regions: a scalable gradient in mineral content (mimicking the scale of native gradient), uniaxially aligned channels (mimicking the scale of native tendon fascicles), and a highly porous HAp/PLGA inverse opal (mimicking the scale and structure of trabecular bone). Cell culture experiments showed that ASCs could be uniformly distributed inside the scaffold with a constant proliferation rate and high cell viability. Immunocytochemistry results demonstrated that the ASCs were able to achieve graded tenogenic and osteogenic differentiation along the mineral gradient with monotonically changing mechanical properties. As aforementioned, there are a variety of other extracellular matrix in the insertion site. Since a gradient in cell phenotype was established in the mineral-graded area of the current study, these cells would likely interact with each other and facilitate the restoration of functional attachment by secretion of suitable extracellular matrix. We hypothesize that the biomimetic hierarchical scaffolds can direct the production of aligned,

unmineralized collagen fibrils in the top region, graded mineralization of collagen in the middle region, and bone regeneration in the bottom region. All three regions will work together to enhance the formation of a mechanically functional tendon-to-bone interface. In a follow-up study, we will test the *in vivo* efficacy of the hierarchical scaffolds in a rotator cuff animal model to promote functional tendon-to-bone attachment.

Supplementary Material

Refer to Web version on PubMed Central for supplementary material.

Acknowledgements

C.Z. and S.P. contributed equally to this work. This work was supported in part by a grant from the National Institutes of Health (R01 AR060820) and startup funds from the Georgia Institute of Technology (to Y.X.).

References

[1]. Genin GM, Thomopoulos S, Nat. Mater 2017, 16, 607. [PubMed: 28541313]

[2]. Schwartz AG, Pasteris JD, Genin GM, Daulton TL, Thomopoulos S, PLoS One 2012, 7, e48630. [PubMed: 23152788]

[3]. Wopenka B, Kent A, Pasteris JD, Yoon Y, Thomopoulos S, Appl. Spectrosc 2008, 62, 1285. [PubMed: 19094386]

[4]. Deymier-Black AC, Pasteris JD, Genin GM, Thomopoulos S, J. Biomech. Eng 2015, 137, 1110051.

[5]. Rossetti L, Kuntz LA, Kunold E, Schock J, Müller KW, Grabmayr H, Stolberg-Stolberg J, Pfeiffer F, Sieber SA, Burgkart R, Bausch AR, Nat. Mater 2017, 16, 664. [PubMed: 28250445]

[6]. Lu HH, Thomopoulos S, Annu. Rev. Biomed. Eng 2013, 15, 201. [PubMed: 23642244]

[7]. Patel S, Gualtieri AP, Lu HH, Levine WN, Ann. N. Y. Acad. Sci 2016, 1383, 97. [PubMed: 27750374]

[8]. Galatz LM, Sandell LJ, Rothermich SY, Das R, Mastny A, Havlioglu N, Silva MJ, Thomopoulos S, J. Orthop. Res 2006, 24, 541. [PubMed: 16456829]

[9]. Galatz LM, Ball CM, Teefey SA, Middleton WD, Yamaguchi K, J. Bone Joint Surg. Am 2004, 86A, 219.

[10]. Yang PJ, Temenoff JS, Tissue Eng. Part B Rev 2009, 15, 127. [PubMed: 19231983]

[11]. Seidi A, Ramalingam M, Elloumi-Hannachi I, Ostrovidov S, Khademhosseini A, Acta Biomater 2011, 7, 1441. [PubMed: 21232635]

[12]. Chen FM, Liu X, Prog. Polym. Sci 2016, 53, 86. [PubMed: 27022202]

[13]. Dormer NH, Berkland CJ, Detamore MS, Ann. Biomed. Eng 2010, 38, 2121. [PubMed: 20411333]

[14]. Zhang X, Bogdanowicz D, Erisken C, Lee NM, Lu HH, J. Shoulder Elbow Surg 2012, 21, 266. [PubMed: 22244070]

[15]. Lu HH, Subramony SD, Boushell MK, Zhang X, Ann. Biomed. Eng 2010, 38, 2142. [PubMed: 20422291]

[16]. Liu W, Lipner J, Xie J, Manning CN, Thomopoulos S, Xia Y, ACS Appl. Mater. Interfaces 2014, 6, 2842. [PubMed: 24433042]

[17]. Lipner J, Liu W, Liu Y, Boyle J, Genin GM, Xia Y, Thomopoulos S, J. Mech. Behav. Biomed. Mater 2014, 40, 59. [PubMed: 25194525]

[18]. Lipner J, Shen H, Cavinatto L, Liu W, Havlioglu N, Xia Y, Galatz LM, Thomopoulos S, Tissue Eng. Part A 2015, 21, 2766. [PubMed: 26414599]

[19]. Hu Y, Birman V, Demyier-Black A, Schwartz AG, Thomopoulos S, Genin GM, Biophys. J 2015, 108, 431. [PubMed: 25606690]

[20]. Loghem JV, Yutskovskaya YA, Philip Werschler W, J. Clin. Aesthet. Dermatol 2015, 8, 38.

[21]. Gentile P, Chiono V, Carmagnola I, Hatton PV, Int. J. Mol. Sci 2014, 15, 3640. [PubMed: 24590126]

[22]. Macrí-Pellizzeri L, Pelacho B, Sancho A, Iglesias-García O, Simón-Yarza AM, Soriano-Navarro M, González-Granero S, García-Verdugo JM, De-Juan-Pardo EM, Prosper F, Tissue Eng. Part A 2015, 21, 1633. [PubMed: 25668195]

[23]. Lee J, Abdeen AA, Zhang D, Kilian KA, Biomaterials 2013, 34, 8140. [PubMed: 23932245]

[24]. Choi SW, Zhang Y, Thomopoulos S, Xia Y, Langmuir 2010, 26, 12126. [PubMed: 20450216]

[25]. Kim HL, Jung GY, Yoon JH, Han JS, Park YJ, Kim DG, Zhang M, Kim DJ, Mater. Sci. Eng. C 2015, 54, 20–25.

[26]. Zhang YS, Zhu C, Xia Y, Adv. Mater 2017, 29, 1701115.

[27]. Screen HR, Lee DA, Bader DL, Shelton JC, Proc. Inst. Mech. Eng. H 2004, 218, 109. [PubMed: 15116898]

[28]. Zhang H, Tang J, Zhang L, An B, Qin L-C, Appl. Phys. Lett 2008, 92, 173121.

[29]. Pongkitwitoon S, Uzer G, Rubin J, Judex S, Sci. Rep 2016, 6, 34791. [PubMed: 27708389]

[30]. Dai R, Wang Z, Samanipour R, Koo KI, Kim K, Stem Cells Int 2016, 2016, 6737345. [PubMed: 27057174]

[31]. Shen H, Gelberman RH, Silva MJ, Sakiyama-Elbert SE, Thomopoulos S, PLoS One 2013, 8, e77613. [PubMed: 24155967]

[32]. Nonoyama T, Wada S, Kiyama R, Kitamura N, Mredha MTI, Zhang X, Kurokawa T, Nakajima T, Takagi Y, Yasuda K, Gong JP, Adv. Mater 2016, 28, 6740. [PubMed: 27184968]

[33]. Gao X, Song J, Ji P, Zhang X, Li X, Xu X, Wang M, Zhang S, Deng Y, Deng F, Wei S, ACS Appl. Mater. Interfaces 2016, 8, 3499. [PubMed: 26756224]

[34]. Guo J, Chan K-M, Zhang J-F, Li G, Exp. Cell Res 2016, 341, 1. [PubMed: 26794903]

[35]. Xu J, Li Z, Hou Y, Fang W, Am. J. Transl. Res 2015, 7, 2527. [PubMed: 26885254]

[36]. Shukunami C, Takimoto A, Oro M, Hiraki Y, Dev. Biol 2006, 298, 234. [PubMed: 16876153]

[37]. Li Y, Ramcharan M, Zhou Z, Leong DJ, Akinbiyi T, Majeska RJ, Sun HB, Sci. Rep 2015, 5, 13149. [PubMed: 26289033]

[38]. Gregory CA, Gunn WG, Peister A, Prockop DJ, Anal. Biochem 2004, 329, 77. [PubMed: 15136169]

[39]. Gersbach CA, Le Doux JM, Guldberg RE, García AJ, Gene Ther 2006, 13, 873. [PubMed: 16496016]

[40]. Wegner KA, Keikhosravi A, Eliceiri KW, Vezina CM, J. Histochem. Cytochem 2017, 65, 479. [PubMed: 28692327]

[41]. Bensimon-Brito A, Cardeira J, Dionísio G, Huysseune A, Cancela ML, Witten PE, BMC Dev. Biol 2016, 16, 2. [PubMed: 26787303]

[42]. Dickhut A, Pelttari K, Janicki P, Wagner W, Eckstein V, Egermann M, Richter W, J. Cell. Physiol 2009, 219, 219. [PubMed: 19107842]

[43]. Gan TX, Taniai S, Zhao G, Huang C, Velenosi TJ, Urquhart BL, Karmazyn M, FASEB 2013, 27, 386.

[44]. Wright J, Jones E, Mod. Pathol 2001, 14, 717. [PubMed: 11455005]

[45]. Kalantari F, Miao D, Emadali A, Tzimas GN, Goltzman D, Vali H, Chevet E, Auguste P, Mod. Pathol 2007, 20, 357. [PubMed: 17334330]

[46]. Russell JN, Clements JE, Gama L, PLoS One 2013, 8, e73849. [PubMed: 24023909]

[47]. Mack E, Neubauer A, Brendel C, Cytometry A 2007, 71, 404. [PubMed: 17431883]

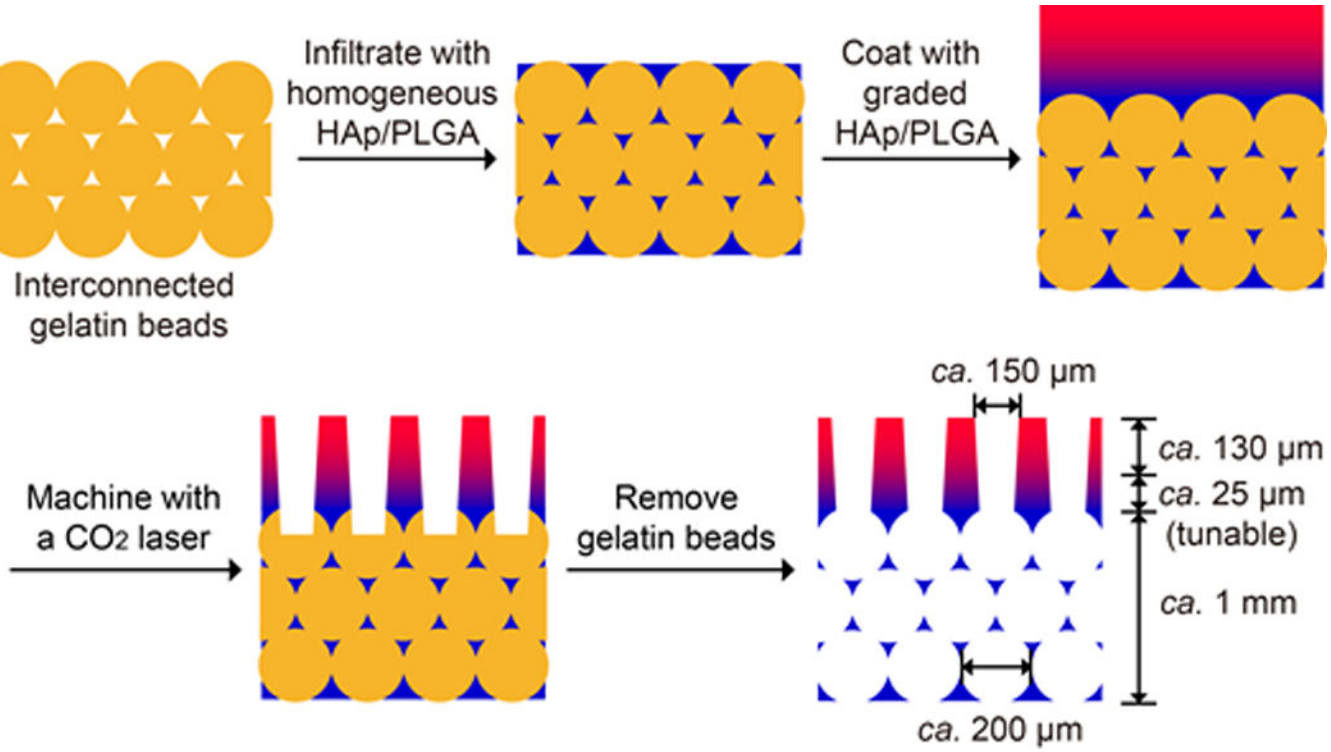

Scheme 1.

Schematic illustration showing the fabrication of a hierarchically structured scaffold for tendon-to-bone repair.

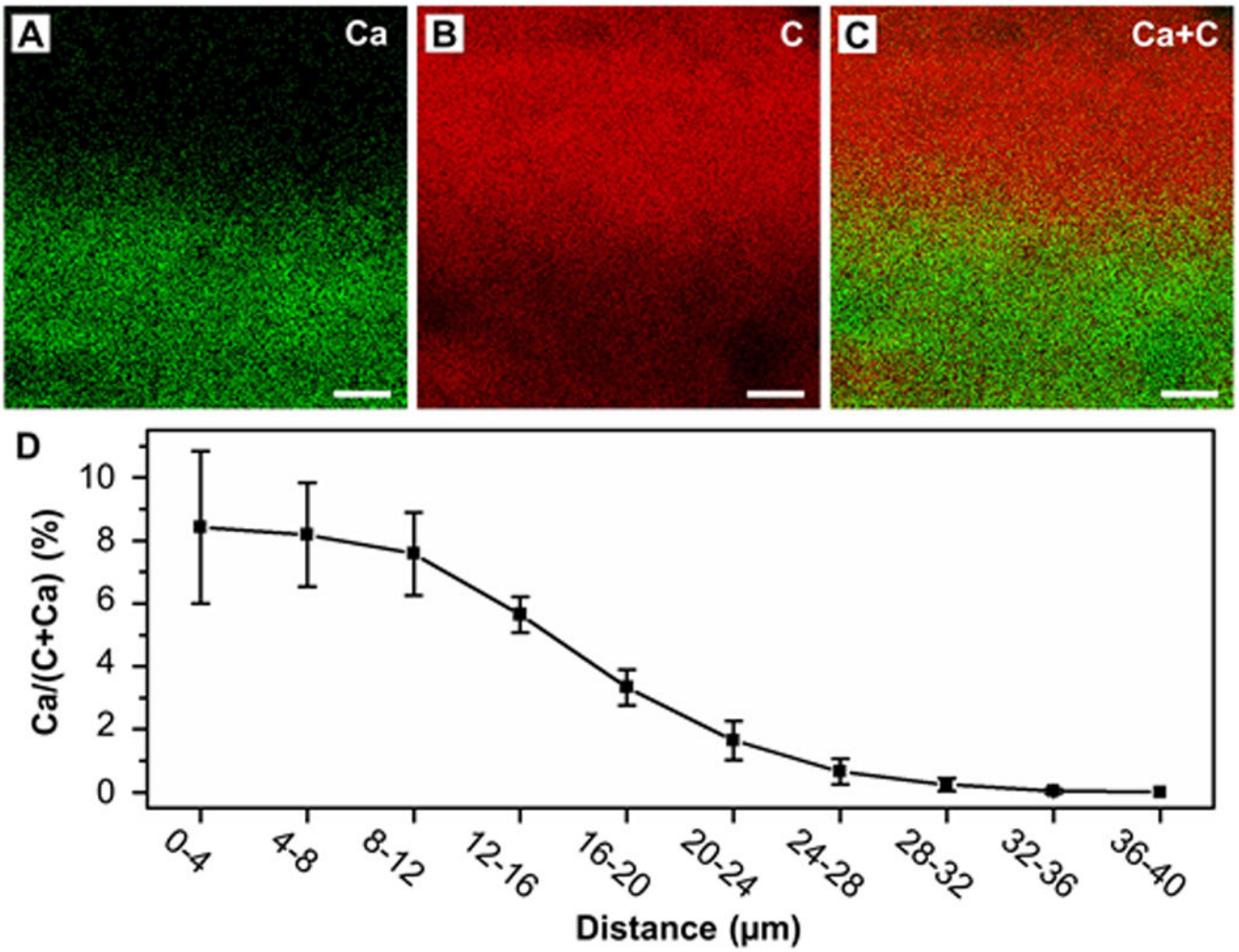

Figure 1.

EDX mapping of elemental distributions recorded from the cross-section of a graded HAp/PLGA scaffold prior to removal of the template. (A−C) Graded distributions of (A) calcium, (B) carbon, and (C) calcium + carbon. Scale bars: 5 μm. (D) Quantification of calcium content along the vertical direction ($n = 3$), where the x axis indicates the distance from the location with the highest mineral content.

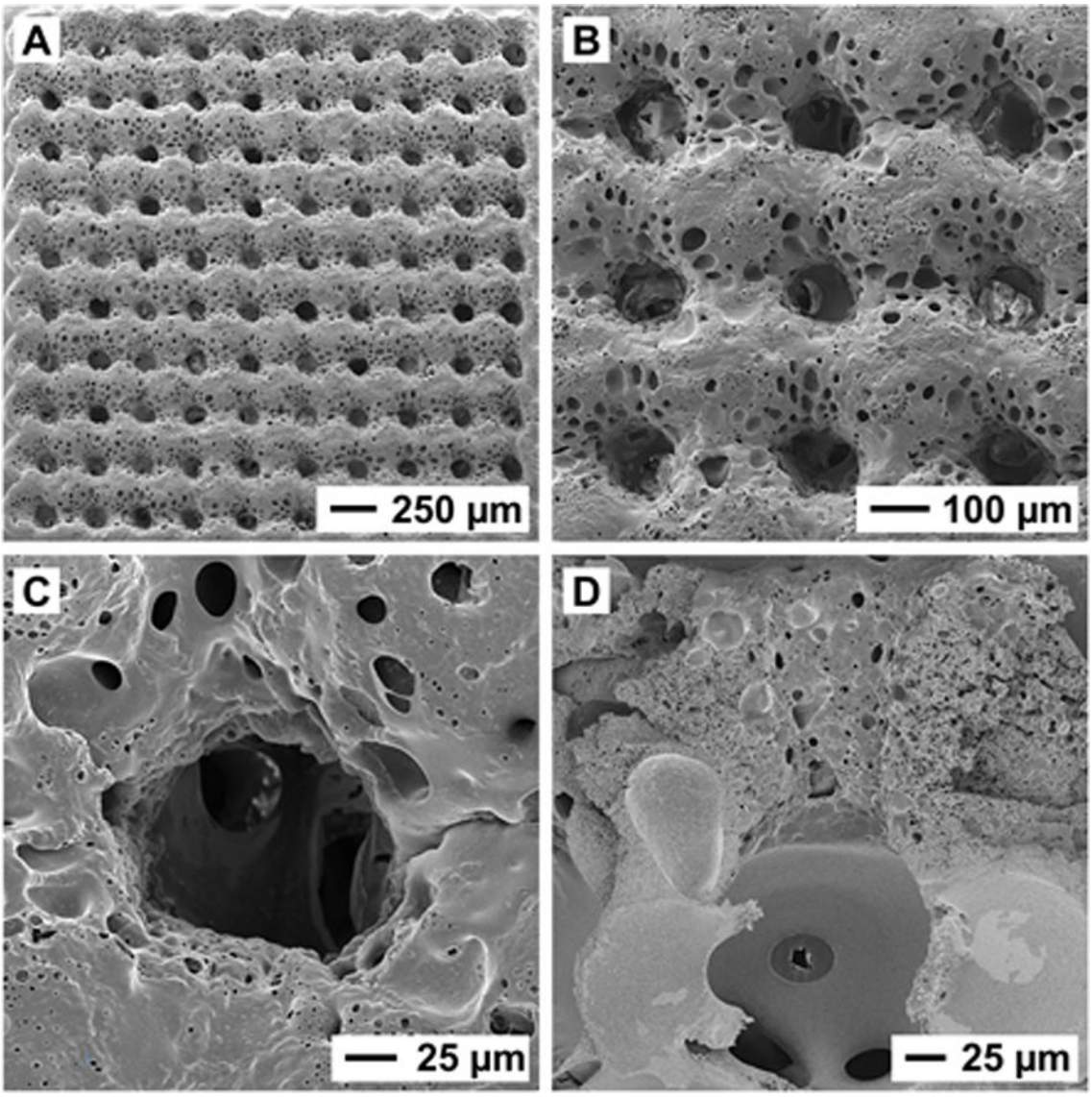

Figure 2.

(A, B) SEM images of a hierarchical scaffold after removal of the template. (C) Higher magnification image showing the morphology of an individual channel. (D) Cross-sectional image taken from an individual channel, showing the interconnectivity between the three different phases.

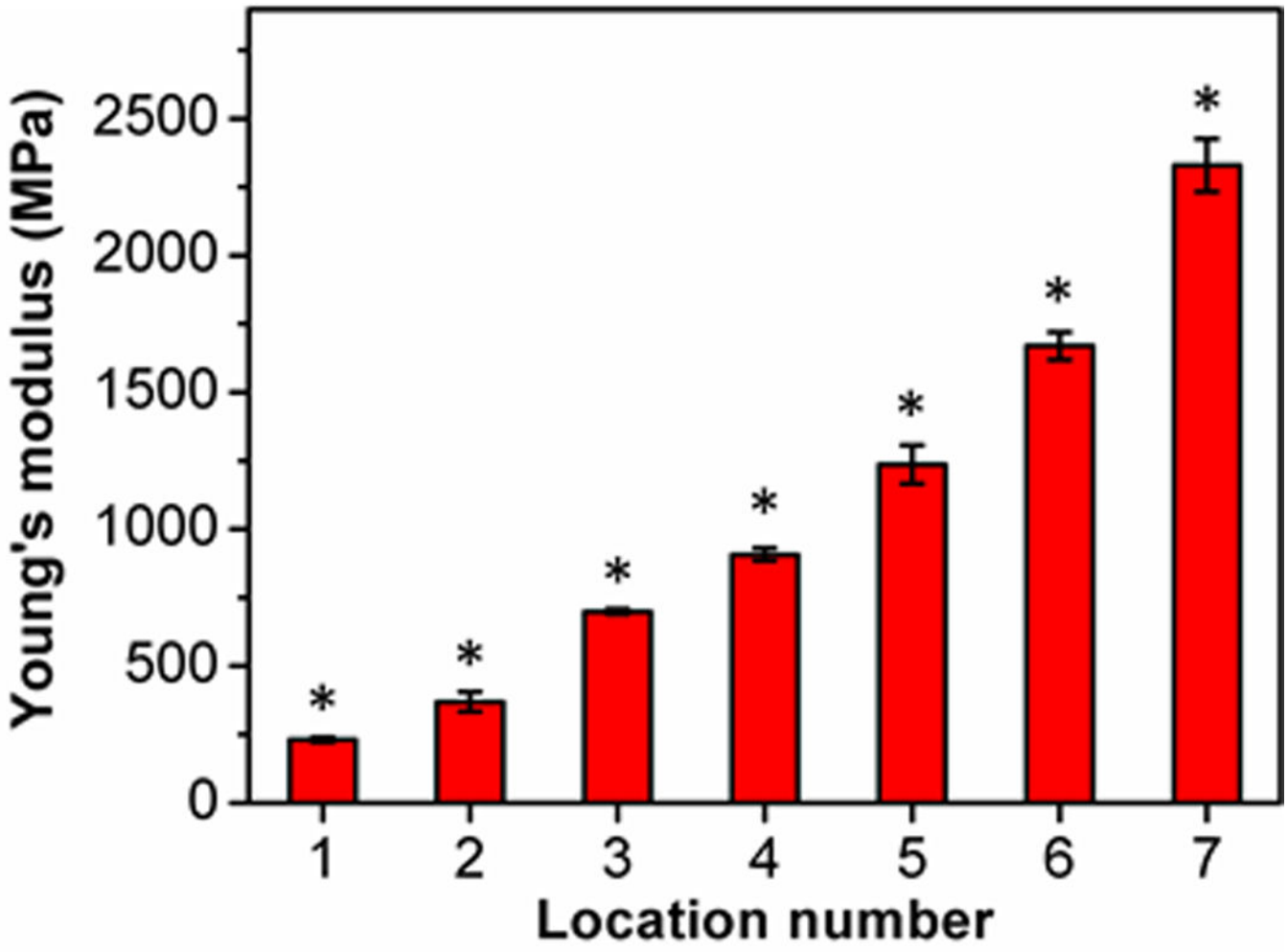

Figure 3.

Local Young's modulus along the mineral gradient in the hierarchically structured scaffolds. The mineral gradient was divided into seven locations ($n = 6$), and the location numbers 1 and 7 represent the unmineralized and highly-mineralized regions, respectively. Significant differences are indicated by * over the bars ($p < 0.05$).

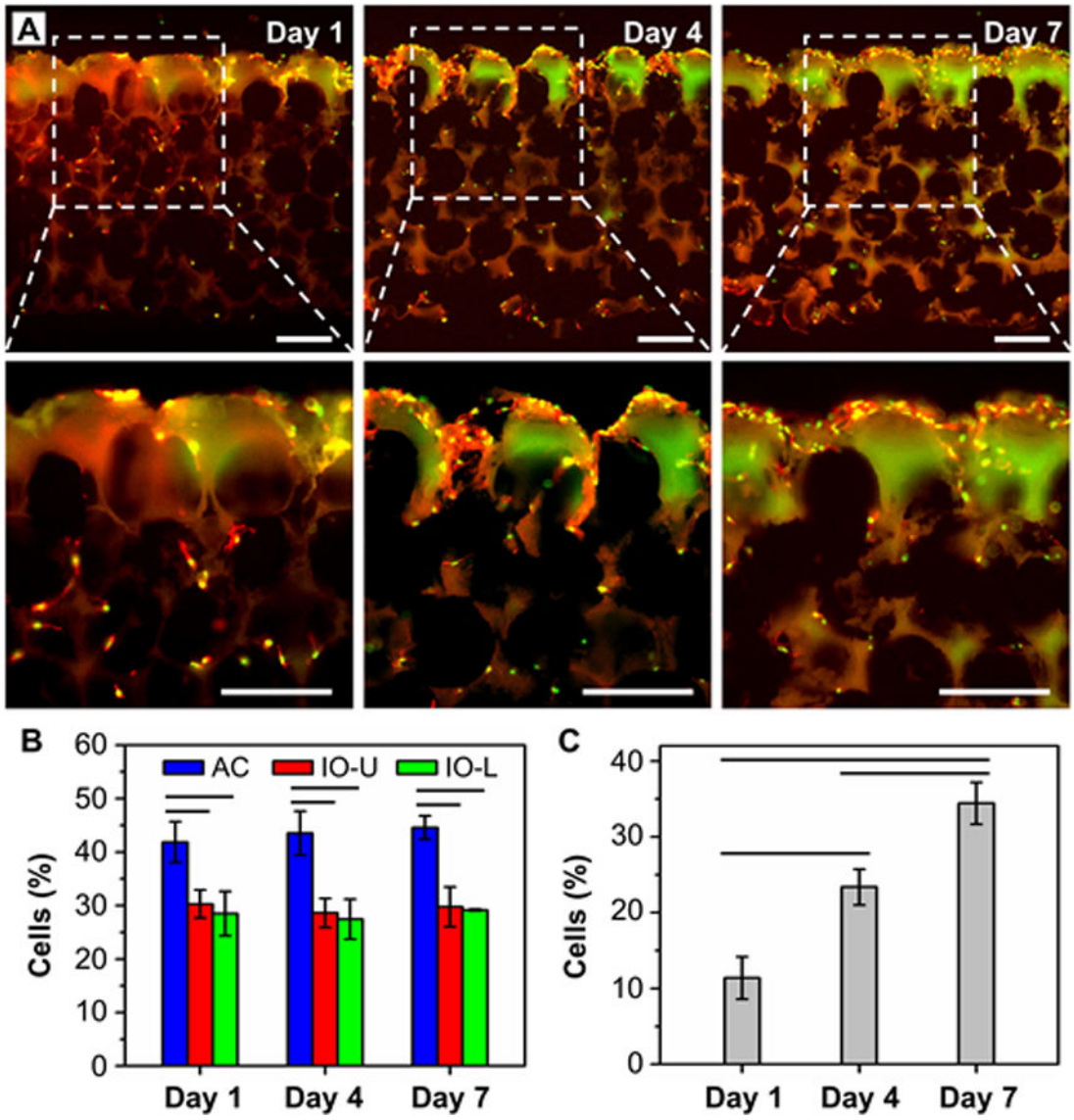

Figure 4.

Distribution and morphology of ASCs inside the hierarchical scaffolds at day 1, 4, and 7 post cell seeding. (A) Superimposed fluorescence images showing the distribution of ASCs. The cytoskeletal F-actin of ASCs was labeled with phalloidin (red), whereas the nuclei were counterstained with DAPI (green). Magnified images corresponding to the regions boxed in (A) are also presented. Scale bars: 250 μm. (B) Quantification of cell distribution. The percentage of cells in each region relative to the total number of cells in the entire sectioned scaffold is shown ($n = 3$). (C) Quantification of cell morphology in the inverse opal region. The percentage of rounded cells relative to the total number of cells is presented ($n = 3$). Significant differences are indicated by lines over the bars ($p < 0.05$).

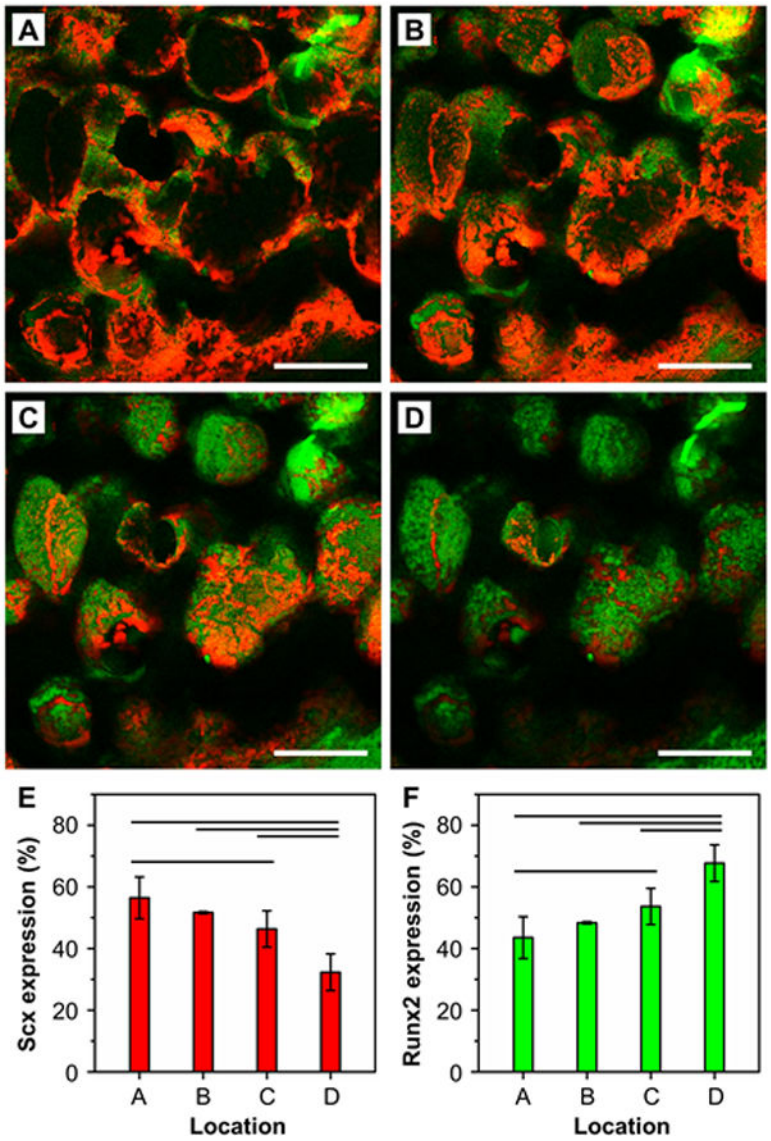

Figure 5.

Scx (red) and Runx2 (green) staining of ASCs seeded in the hierarchical scaffold after 28 days of culture. (A) Unmineralized region, (B) transitional region with less mineral content, (C) transitional region with more mineral content, and (D) highly-mineralized region. Scale bars: 200 μm. (E, F) Semi-quantitative analysis of the expressions of (E) Scx and (F) Runx2 ($n = 6$). Significant differences are indicated by lines over the bars ($p < 0.05$).